Physica Scripta

INCLUSIVE PUBLISHING
TRUSTED SCIENCE

PAPER • OPEN ACCESS

$Ti_3C_2O_2$ MXene single-layer as a nanoscale transport device

To cite this article: Ünal Özden Akkuş *et al* 2024 *Phys. Scr.* **99** 025977

View the article online for updates and enhancements.

You may also like

- Nanoengineering of MXene-Based Field-Effect Transistor Gas Sensors: Advancements in Next-Generation Electronic Devices
P. Baraneedharan, D. Shankari, A. Arulraj et al.
- Synthesis and applications of MXene-based composites: a review
Umar Noor, Muhammad Furqan Mughal, Toheed Ahmed et al.
- MXenes hierarchical architectures: electromagnetic absorbing, shielding and devices
Qiang-qiang Wang, Wen-qiang Cao and Mao-sheng Cao

This content was downloaded from IP address 194.27.6.19 on 07/02/2024 at 05:54

Physica Scripta

PAPER

$Ti_3C_2O_2$ MXene single-layer as a nanoscale transport device

Ünal Özden Akkuş[1], Erdem Balcı[2] and Savas Berber[1]

[1] Department of Physics, Gebze Technical University, Gebze, Kocaeli 41400, Turkey
[2] Gazi University, Faculty of Medicine, Department of Nuclear Medicine, Ankara, Turkey

E-mail: savasberber@gtu.edu.tr

Keywords: MXene, field effect transistor, NEGF, Ti3C2O2, Ti2CO2, quantum transport

OPEN ACCESS

RECEIVED
29 November 2023

REVISED
3 January 2024

ACCEPTED FOR PUBLICATION
16 January 2024

PUBLISHED
25 January 2024

Original content from this work may be used under the terms of the Creative Commons Attribution 4.0 licence.

Any further distribution of this work must maintain attribution to the author(s) and the title of the work, journal citation and DOI.

Abstract

We considered $Ti_3C_2O_2$ MXene single-layers with stepped edges as a nanoscale field effect transistor (FET) device. Our model device contains stepped edges at the interface of $Ti_3C_2O_2$ and Ti_2CO_2 segments, and a top gate. We suggest that Ti_2CO_2 semiconducting device region can be obtained by etching the central part of a $Ti_3C_2O_2$ single-layer. We determined the device characteristic of the proposed device in non-equilibrium Green's function (NEGF) calculations and observed the transistor behavior. The current through the device is controllable by the total amount of accumulated charge on the gate electrode. Our findings should be applicable to a large number of MXenes: Starting from $M_3C_2O_2$ MXene single-layers, nanoscale FETs could be produced using conventional mask and etching lithography techniques.

1. Introduction

MXenes [1] are two-dimensional (2D) material family of transition metal carbides and nitrides with desirable properties for nanoscale device applications [2–4]. The 2D confinement of ultra-thin materials, such as graphene [5, 6], provide a natural geometry to improve field-effect transistor (FET) device characteristics [7]. As an alternative, MXenes found several applications [8–12] taking advantage of their flexible 2D structure. The electronic structure of MXenes can be tuned by surface chemical modifications in addition to the stoichiometry [13–15]. Both metallic and semiconducting segments of a nanodevice could be made of MXenes that could be seamlessly adjoined.

MXenes are produced by separating the layers of three-dimensional $M_{n+1}AX_n$ (n = 1, 2, 3) or MAX crystals [16, 17], where 'M' represents the early transition metals, 'A' the elements of the A group, and 'X' carbon or nitrogen atoms. Etching group A elements of the MAX crystal [18] results in F, O, or OH terminated 2D MXene layers [19]. Usually, both O and F terminations occur simultaneously on the same MXene layer [16, 19]. The termination group ratio in a sample is varied by the choice of the etching agent [19, 20]. Besides, the surface termination may be modified [21] after de-functionalization [22] of the layer. As we expect that an O-terminated MXene device is air-stable, we concentrate on O-terminated MXenes.

Ti-based MXenes are experimentally the most accessible among the MXenes. An FET, based on Ti_3C_2 MXene micropatterns has been shown to be a highly sensitive biosensor [23]. MXene-graphene FET device was shown to detect both influenza and 2019-nCoV viruses. In this combination, the high chemical sensitivity of MXene and the large-area, high-quality structure of graphene are merged to create an ultra-sensitive virus transduction material [24]. Organic field effect transistors (OFETs) with Ti_2CT_x electrode and pentacene channel were produced for device applications [25]. It was found that Ti_2CT_x is a promising electrode for high-performance OFET applications. The use of $Ti_3C_2T_x$ MXene as a source electrode offers many opportunities for high-performance organic vertical transistors and photovoltaic devices due to its ultra-thin thickness and natural oxidation [26]. Hybridization of $Ti_3C_2T_x$ MXene with Ag nanoparticles on an FET platform was found to be efficient for the detection of dangerous H_2S gas [27]. Functionalized $Ti_3C_2T_x$-MXene based field effect transistors were shown to be capable of efficient biosensing [28], and volatile compound detection [29]. In addition, MXene field effect transistors were utilized in the detection of Ag ion [30] and alkali sensing in harsh environments [31]. MXene-based field-effect transistors are now considered as efficient sensing medium [32].

© 2024 The Author(s). Published by IOP Publishing Ltd

Here, we propose a new MXene FET device that could be achieved by lithography techniques. A single layer with a common carbon skeleton can provide essential ingredients for a field effect transistor. Starting from metallic $Ti_3C_2O_2$ single-layer, a narrow semiconducting Ti_2CO_2 device region can be obtained after selectively etching by lithography. The model device contains stepped edges at the interface of $Ti_3C_2O_2$ and Ti_2CO_2 segments. Although there are several candidates for the transition metal M, we have chosen Ti since Ti-based MXenes are readily used for FET applications [33].

We calculated the electrical transport characteristic of the model device in quantum transport regime using the non-equilibrium Green's function (NEGF) technique. In our model FET, a charge layer was placed above the MXene layer to simulate the top gate that creates the electric field and promote the conduction channel in the underlying MXene layer. Although the tunneling region and electrodes are structurally compatible with the common MXene backbone, the stepped edges and the incompatibility of the electronic levels are major scattering mechanisms. The potential jumps at the contacts due to drain-source voltage (V_{DS}) values of up to 0.05 V lead to additional scattering. We keep the bias voltages in the low-bias regime to prevent numeric instabilities in our NEGF simulations of our model gated device.

2. Methods

We performed density functional theory (DFT) structure optimization, electronic structure, and quantum transport calculations in the SIESTA [34] computer package. Exchange-correlation energy was handled by the Perdew–Burke–Ernzerhof (PBE) functional in the Generalized Gradient Approximation (GGA) [35]. The interactions between the core and the valence electrons were described by norm-conserving Troullier–Martins pseudopotentials [36, 37]. The strong electron-electron interactions in the localized atomic shells of Ti were incorporated by Dudarev's GGA+U method [38]. The U value of 3.5 eV was taken from previous studies [39–41]. To calculate the two-dimensional MXene, a vacuum space larger than 30 Å in the perpendicular direction was placed between the layers to prevent the interaction between adjacent layers. The electron density was expressed on a real space grid that corresponds to a plane wave cut-off energy of 300 Ry. The electronic temperature was set to 300 K. The wavefunctions were expressed by a split-type double-ζ basis set, generated with the energy shift of 0.05 eV as implemented in the SIESTA code. Geometry optimization calculations were pursued until all force components are less than 0.01 eV/Å. The self-consistent field (SCF) cycles were continued until the density matrix elements changed no more than 10^{-4}. Transport calculations were performed in the TranSIESTA [42, 43] module using the non-equilibrium Green's function (NEGF) technique [44]. A dense $101 \times 21 \times 1$ k-point sampling was used in transport calculations. In order to improve the convergence in the transport calculations, real space grid cut-off energy was reduced to 200 Ry in TranSIESTA runs. We utilized Landauer-Buttiker equation in the NEGF approach [45] and computed the generated current $I(V_{DS})$ by

$$I(V_{DS}) = \frac{2e^2}{h}\int_{-\infty}^{\infty} T(E, V_{DS})[f_L(E-\mu_L) - f_R(E-\mu_R)]dE, \quad (1)$$

where the $T(E, V_{DS})$ is the transmission probability of electrons at energy E under the applied drain-source voltage V_{DS}. The $f_{L(R)}$ is the Fermi–Dirac distribution function and $\mu_{L(R)}$ is the chemical potential of left(right) electrode.

3. Results

Our model transistor device, shown in figure 1, consists of infinite $Ti_3C_2O_2$ single-layer etched in the central region. The tetragonal unit cell is utilized for the single-layer. After etching, the scattering region becomes Ti_2CO_2 MXene with stepped edges. Around the central scattering region, the electrodes are formed by repeating the tetragonal unit cell of $Ti_3C_2O_2$ along the semi-infinite $+x$ and $-x$-directions. As indicated in figure 1, small part of $Ti_3C_2O_2$ electrode material was included in the scattering region. A unit of the scattering region includes 18 tetragonal unit cells of Ti_2CO_2 and 2 tetragonal unit cells of $Ti_3C_2O_2$. This scattering unit and the electrodes are repeated periodically along the y-axis with the lattice vector length of 5.33 Å. Source and drain are placed such that the conduction is along the x-axis. In our calculations, the gate is simulated by a charged box of 3 Å thickness placed above the gated region of the MXene, shown in figure 1. The total charge of the gate electrode is distributed uniformly over this 3 Å thick box.

Starting from the available structural data, we optimized the atom coordinates and lattice constants of $Ti_3C_2O_2$. Our calculated hexagonal lattice constant value of $a \approx 3.098$ Å for $Ti_3C_2O_2$ is in good agreement with previous works [13, 46]. The scattering region augmented by the electrodes was fully relaxed in periodic boundary conditions before the NEGF transport calculations. The electrode atoms were constrained during the

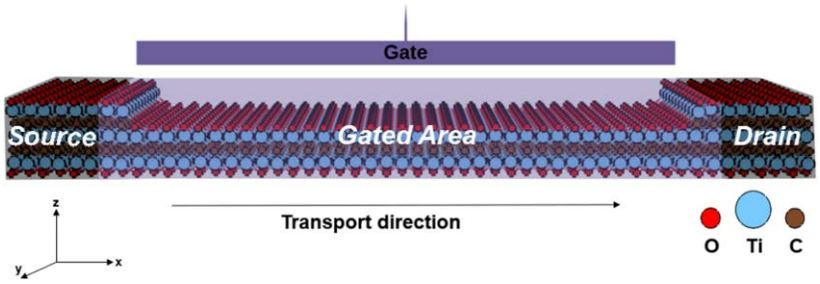


Figure 1. Model device structure. The drain and source electrodes are made up of $Ti_3C_2O_2$, while the scattering region consists of both $Ti_3C_2O_2$ and Ti_2CO_2 stepped edge. Blue, brown, and red spheres represent Ti, C, and O atoms, respectively. The top gate is depicted above the scattering region.

structure optimizations while the atoms in the gated region, shown in figure 1, was free to move. The electrodes were optimized independently.

While $Ti_3C_2O_2$ electrodes are metallic, Ti_2CO_2 MXene of the scattering region is semiconducting [47]. The electronic structure of $Ti_3C_2O_2$ shown in figure 2(a) has Ti and C related states around the Fermi level E_F. However, the valence bands of Ti_2CO_2, shown in figure 2(b), are formed by the mixed states of Ti, C, and O. Although the scattering region is seamlessly connected to the electrodes, the transmission is not perfect due to level mismatch, and the step edges may create additional scattering.

The energy-resolved transmission $T(E)$ of the device is shown in figure 3 for the gate electrode's total charge values of 0.0, 0.5, and 1.0 e. The energy values are with respect to the average chemical potential $(\mu_L + \mu_R)/2$ of the electrodes. The transmission values are averaged over 21 k_y-points to calculate $T(E)$ values in figure 3 since the device is periodic along the y-axis. In figure 3, only the V_{DS} values of 0.01, 0.03, and 0.05 V are selected to show the trend.

The bias energy window of $\pm eV_{DS}/2$ is denoted by vertical blue lines in figure 3 to indicate the levels contributing to the total current: Under the V_{DS}, the energy levels between $\pm eV_{DS}/2$ contribute to the current. The total current is proportional to the integrated $T(E)$ over the energy window of eV_{DS}. The vanishing $T(E)$ values around the average chemical potential indicates a transport gap of 0.65 eV when the gate electrode is not charged. This gap is compatible with the gap in the electronic bands of an infinite Ti_2CO_2 along the transport direction, presented in figure 2(b). As the bias voltages are small, the transport gaps are almost the same in all panels of figure 3 for uncharged gate electrode. The transmission curves in figure 3 are shifted to the right towards higher energies when the gate acquires excess charge values of 0.5, and 1.0 e. Apparently, the top gate shifts the energy levels of the scattering region up, pushing some conducting states into $\pm eV_{DS}/2$ bias window. The transport gap is pushed to higher energy values while the value of the gap essentially remains the same.

The transmission between the conduction band levels are through Ti states. But, the transmission between valence levels are via Ti, C, and O mixed states. Therefore, $T(E)$ values above the reference level $(\mu_L + \mu_R)/2$ are higher than $T(E)$ at negative energies.

Transmission $T(E)$ becomes slightly higher as V_{DS} gets larger. More states contribute to the current as the bias window expands at higher V_{DS} values. In addition, $T(E)$ values in the bias window increase as the gate charge rises from 0.5 e to 1.0 e. Therefore, higher current values are expected for higher gate excess charges values.

The calculated I_{DS} values for our model $Ti_3C_2O_2/Ti_2CO_2/Ti_3C_2O_2$ device are presented as a function of the total charge on the gate electrode in figure 4 for the drain-source voltages of 0.01, 0.02, 0.03, 0.04, and 0.05 V. The current values are given per 5.33 Å wide MXene single-layer. As expected, the higher V_{DS} values lead to higher current values since more states contribute to the total current as the bias window widens. Stemming from the features of $T(E)$ in figure 3, the current values increase with increasing gate charge. The threshold gate excess charge seems to be 0.4 e for our model device to have nonzero current. The current then saturates with the gate charge above 1.0 e. The current profile in figure 4 indicates that our model device show a transistor characteristic. The excess charge on the gate creates an electric field on the device. Thus, the current is controlled by the electric field created by the excess charge of the top gate.

There are no scattering region electronic states to transmit the charge carriers in the absence of a gate voltage. The transmission gap is thus the result of the electronic energy gap of the scattering region, which consists of Ti_2CO_2 MXene. As GGA functional underestimates the energy gaps, higher transmission gaps are expected with hybrid functionals. However, the main features in transmission spectra are related to occupied bands, and the band shapes in MXenes are not altered by hybrid functionals [48].

The gate charge in our model top gated nanoscale field effect transistor pulls the electrons towards the edges between the conducting MXene electrodes and the semiconducting MXene scattering region. Thus, the edge

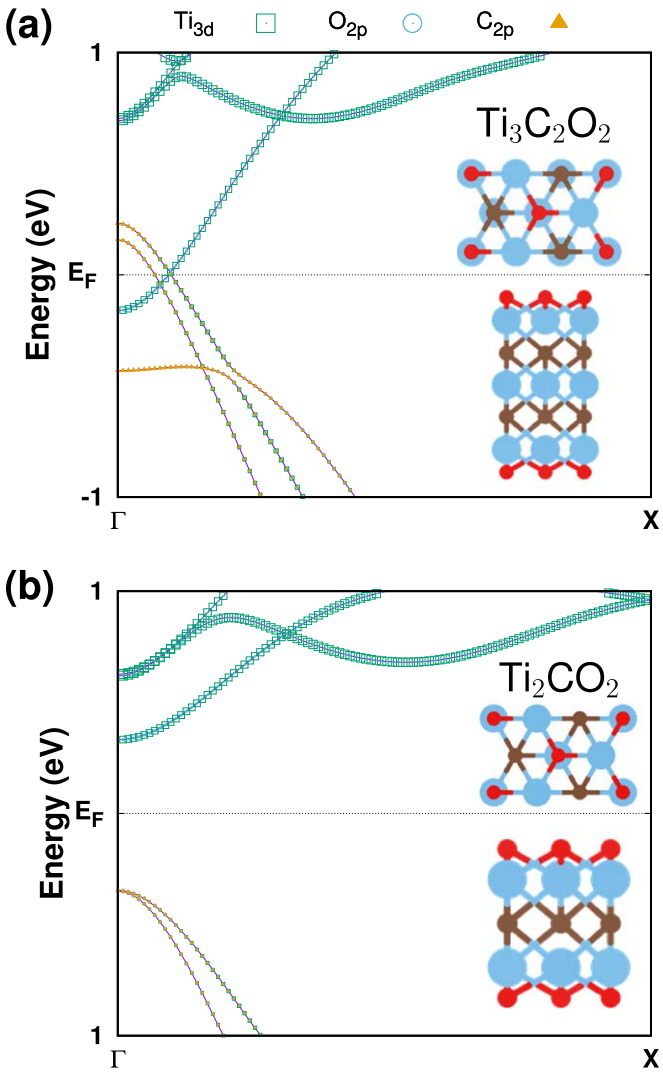


Figure 2. The atomic orbital resolved electronic band structures of $Ti_3C_2O_2$, and Ti_2CO_2 along the transport direction are shown in (a), and (b), respectively. The size of the data points are proportional to the wavefunction projection on the specified atomic orbital. Top and side views of two-dimensional $Ti_3C_2O_2$, and Ti_2CO_2 MXenes unit cells are shown as insets.

states become occupied and contribute to the conduction. The transmission channel stems from the edges that originally block the transmission in a non-gated system. In our simulations, the excess charge on the gate is the controlled parameter to increase the electric field on the scattering region. Our results in figure 4 indicate that the current increases with increasing electric field under a constant bias voltage. The proposed nanoscale MXene-based FET may extend the sensing applications of current FET devices [28–30, 32] to single molecule detection level and improve the switching time.

The length of the scattering region is 62 Å in our Ti-based model device. Note that the scattering region should be wide enough to develop an electronic energy gap, and prevent tunneling currents. Our results show that an MXene with ≈6 nm long gated processing region is able to show field effect transistor (FET) characteristics. We believe that $Ti_3C_2O_2$ MXene single-layer can be utilized as a transistor using conventional mask and etching lithography techniques. We expect that the real devices longer than 6 nm will have better on/off ratios.

Experimental realization of the model device requires the exfoliation of a single MXene layer, which was achieved to form MXene gate electrodes in metal chalcogenide transistors [49]. Nevertheless, isolating an MXene single layer remains to be a challenge for the fabrication of a nanoscale MXene FET device. However, new synthesis techniques [50, 51] allow the growth of an MXene layer without going through the acid etching process, eliminating the need to separate the layers.

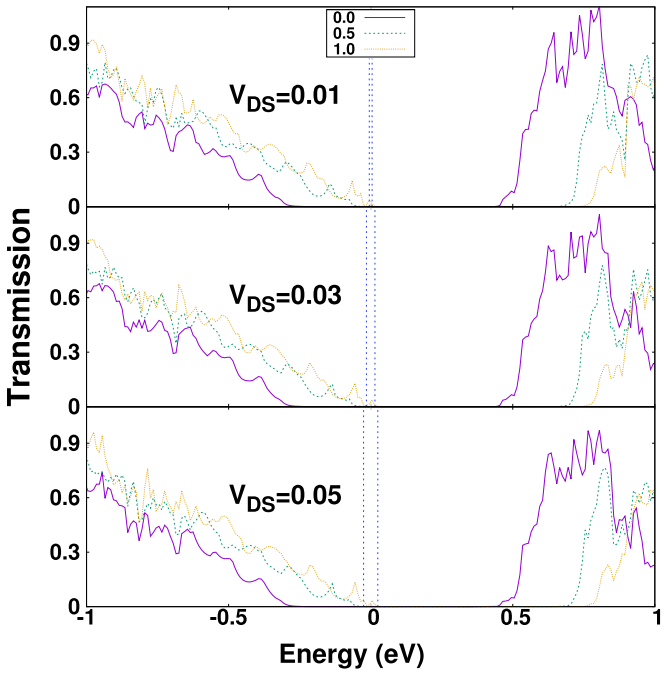


Figure 3. Transmission spectra of the stepped $Ti_3C_2O_2/Ti_2CO_2/Ti_3C_2O_2$ device for $V_{DS} = 0.01, 0.03$, and 0.05 V bias voltage values. Energy is with respect to the average chemical potential $(\mu_L+\mu_R)/2$ of the electrodes. The transmission values are shown for the total gate charge values of 0.0, 0.5, and 1.0 *e*. The vertical blue lines indicate the bias energy window eV_{DS}.

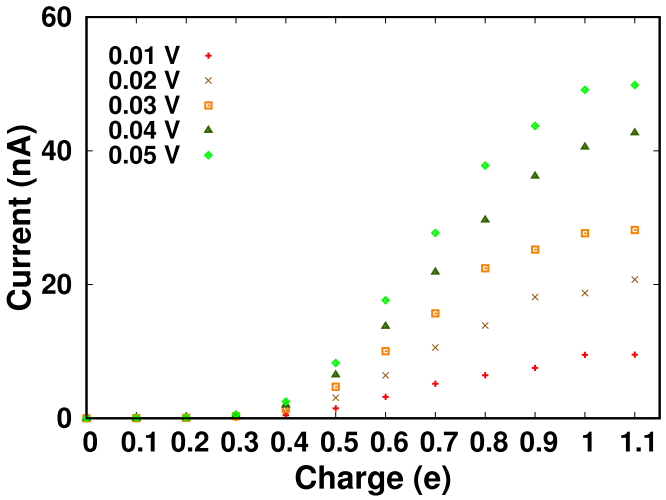


Figure 4. The drain-source current (I_{DS}) in $Ti_3C_2O_2/Ti_2CO_2/Ti_3C_2O_2$ device for the drain-source voltage V_{DS} values of 0.01, 0.02, 0.03, 0.04, and 0.05 V as a function of the total excess charge distributed on the top gate electrode.

4. Summary and conclusion

We considered $Ti_3C_2O_2$ MXene single-layers with stepped edges as a nanoscale field-effect transistor. Our model device consists of $Ti_3C_2O_2$ MXene electrodes and Ti_2CO_2 scattering region, over which a top gate is placed. We determined the device characteristics of the proposed device in non-equilibrium Green's function (NEGF) calculations and observed field-effect transistor behavior of the current control by the gate-produced field. The electronic energy gap of the scattering region leads to a transmission gap because the scattering region has no electronic states at the energy levels of the incoming charge carriers. The charged gate electrode shifts up the energy levels of the scattering region and modifies the transmission values. Thus, the current stems from the valence states pushed into the bias window by the electric field created by the gate. Starting from $Ti_3C_2O_2$ MXene single-layers, nanoscale devices could be produced using lithographic mask and etching techniques. Our results

on model $Ti_3C_2O_2/Ti_2CO_2/Ti_3C_2O_2$ device indicate that a single MXene layer can be utilized to form a field effect transistor.

Acknowledgments

The numerical calculations were performed at TÜBİTAK ULAKBİM, High Performance and Grid Computing Center (TRUBA) resources. This work is part of TÜBİTAK project No. 118F043.

Data availability statement

The data cannot be made publicly available upon publication because no suitable repository exists for hosting data in this field of study. The data that support the findings of this study are available upon reasonable request from the authors.

Conflict of interest

The authors declare no competing financial interests.

ORCID iDs

Erdem Balcı https://orcid.org/0000-0002-9762-6741
Savas Berber https://orcid.org/0000-0003-0949-2614

References

[1] Barsoum M W 2013 *MAX Phases: Properties of Machinable Ternary Carbides and Nitrides* (Wiley)
[2] Zhou Y, Luo K, Zha X, Liu Z, Bai X, Huang Q, Guo Z, Lin C T and Du S 2016 *J. Mater. Chem. C* **120** 17143–52
[3] Zhou Y, Zhai G, Yan T, Huang Q, Guo Z, Lin C T and Du S 2017 *Comput. Mater. Sci.* **138** 175–82
[4] Lai S, Jeon J, Jang S K, Xu J, Choi Y J, Park J H, Hwang E and Lee S 2015 *Nanoscale* **7** 19390–6
[5] Wessely P J, Wessely F, Birinci E, Beckmann K, Riedinger B and Schwalke U 2012 *Physica E* **44** 1132–5
[6] Jena D 2013 *Proc. IEEE* **101** 1585–602
[7] Chhowalla M, Jena D and Zhang H 2016 *Nat. Rev. Mater.* **1** 16052
[8] Ronchi R M, Arantes J T and Santos S F 2019 *Ceram. Int.* **45** 18167–88
[9] Khazaei M, Mishra A, Venkataramanan N S, Singh A K and Yunoki S 2019 *Curr. Opin. Solid State Mater. Sci.* **23** 164–78
[10] Fu Z, Liu Z, Legut D, Germann T C, Si C, Du S, Francisco J S and Zhang R 2019 *J. Phys. Chem. C* **123** 20664–74
[11] Fu Z, Wang N, Legut D, Si C, Zhang Q, Du S, Germann T C, Francisco J S and Zhang R 2019 *Chem. Rev.* **119** 11980–2031
[12] Jiang X, Kuklin A V, Baev A, Ge Y, Ågren H, Zhang H and Prasad P N 2020 *Phys. Rep.* **848** 1–58
[13] Khazaei M, Arai M, Sasaki T, Chung C Y, Venkataramanan N S, Estili M, Sakka Y and Kawazoe Y 2013 *Adv. Funct. Mater.* **23** 2185–92
[14] Khazaei M, Ranjbar A, Arai M, Sasaki T and Yunoki S 2017 *J. Mater. Chem. CJ. Mater. Chem. C* **5** 2488–503
[15] Zhou J, Khazaei M, Ranjbar A, Wang V, Kühne T D, Ohno K, Kawazoe Y and Liang Y 2020 *J. Mater. Chem. C* **8** 5211–21
[16] Naguib M, Kurtoglu M, Presser V, Lu J, Niu J, Heon M, Hultman L, Gogotsi Y and Barsoum M W 2011 *Adv. Mater.* **23** 4248–53
[17] Naguib M, Mashtalir O, Carle J, Presser V, Lu J, Hultman L, Gogotsi Y and Barsoum M W 2012 *ACS Nano* **6** 1322–31
[18] Malaki M, Maleki A and Varma R S 2019 *J. Mater. Chem. A* **7** 10843–57
[19] Hope M A, Forse A C, Griffith K J, Lukatskaya M R, Ghidiu M, Gogotsi Y and Grey C P 2016 *Phys. Chem. Chem. Phys.* **18** 5099–102
[20] Ghidiu M, Lukatskaya M R, Zhao M Q, Gogotsi Y and Barsoum M W 2014 *Nature* **516** 78
[21] Han M, Yin X, Wu H, Hou Z, Song C, Li X, Zhang L and Cheng L 2016 *ACS Appl. Mater. Interfaces* **8** 21011–9
[22] Hart J L, Hantanasirisakul K, Lang A C, Anasori B, Pinto D, Pivak Y, van Omme J T, May S J, Gogotsi Y and Taheri M L 2019 *Nat. Commun.* **10** 522
[23] Xu B, Zhu M, Zhang W, Zhen X, Pei Z, Xue Q, Zhi C and Shi P 2016 *Adv. Mater.* **28** 3333–9
[24] Li Y *et al* 2021 *ACS Omega* **6** 6643–53
[25] Lai S, Jang S K, Cho J H and Lee S 2018 *Nanoscale* **10** 5191–7
[26] Li E, Gao C, Yu R, Wang X, He L, Hu Y, Chen H, Chen H and Guo T 2022 *Nat. Commun.* **13** 2898
[27] Xu Q, Zong B, Li Q, Fang X, Mao S and Ostrikov K K 2022 *J. Hazard. Mater.* **424** 127492
[28] Siva S, Bodkhe G A, Cong C, Hyun Kim S and Kim M 2024 *Chem. Eng. J.* **479** 147492
[29] Zong B, Xu Q and Mao S 2022 *ACS Sens.* **7** 1874–82
[30] Liu C, Wei X, Hao S, Zong B, Chen X, Li Z and Mao S 2021 *Anal. Chem.* **93** 8010–8
[31] Liu C, Hao S, Chen X, Zong B and Mao S 2020 *ACS Appl. Mater. Interfaces* **12** 32970–8
[32] Baraneedharan P, Shankari D, Arulraj A, Sephra P J, Mangalaraja R V and Khalid M 2023 *J. Electrochem. Soc.* **170** 107501
[33] Verger L, Natu V, Carey M and Barsoum M W 2019 *Trends in Chemistry* **1** 656–69
[34] Soler J M, Artacho E, Gale J D, García A, Junquera J, Ordejón P and Sánchez-Portal D 2002 *J. Phys.: Condens. Matter* **14** 2745
[35] Perdew J P, Burke K and Ernzerhof M 1996 *Phys. Rev. Lett.* **77** 3865–8
[36] Troullier N and Martins J L 1991 *Phys. Rev. B* **43** 1993–2006
[37] Kleinman L and Bylander D M 1982 *Phys. Rev. Lett.* **48** 1425–8
[38] Dudarev S L, Botton G A, Savrasov S Y, Humphreys C J and Sutton A P 1998 *Phys. Rev. B* **57** 1505–9
[39] Chakraborty P, Das T, Nafday D, Boeri L and Saha-Dasgupta T 2017 *Phys. Rev. B* **95** 184106

[40] Guo X, Zhang P and Xue J 2016 *J. Phys. Chem. Lett.* **7** 5280–4
[41] Wang D, Gao Y, Liu Y, Jin D, Gogotsi Y, Meng X, Du F, Chen G and Wei Y 2017 *J. Mater. Chem. C* **121** 13025–34
[42] Brandbyge M, Mozos J L, Ordejón P, Taylor J and Stokbro K 2002 *Phys. Rev. B* **65** 165401
[43] Papior N, Lorente N, Frederiksen T, García A and Brandbyge M 2017 *Comput. Phys. Commun.* **212** 8–24
[44] Datta S 2000 *Superlattice. Microst.* **28** 253–78
[45] Landauer R 1970 *Philos. Mag.* **21** 863–7
[46] Li H, Li A, Zhang D, Wu Q, Mao P, Qiu Y, Zhao Z, Yu P, Su X and Bai M 2022 *ACS Omega* **7** 40578–85
[47] Wang T, Li N, Li Y, Kai J J and Fan J 2021 *J. Phys. Chem. C* **125** 82–90
[48] Lee Y, Hwang Y and Chung Y C 2015 *ACS Appl. Mater. Interfaces* **7** 7163–9
[49] Jiao X, Jaewoo S, Jin-Hong P and Sungjoo L 2016 *Adv. Funct. Mater.* **26** 5328–34
[50] Verger L, Xu C, Natu V, Cheng H M, Ren W and Barsoum M W 2019 *Curr. Opin. Solid St. M.* **23** 149–63
[51] Fan Y, Li L, Zhang Y, Zhang X, Geng D and Hu W 2022 *Adv. Funct. Mater.* **32** 2111357